ACS Catalysis

Research Article

pubs.acs.org/acscatalysis

Asymmetric Dual-Catalytic Cascade by Chiral N-Heterocyclic Carbene and Quinuclidine: Mechanism and Origin of Enantioselectivity in Benzofuranone Formation

Yernaidu Reddi and Raghavan B. Sunoj*

Department of Chemistry, Indian Institute of Technology Bombay, Powai, Mumbai 400076, India

Supporting Information

ABSTRACT: Contemporary literature offers a number of interesting examples for asymmetric multicatalytic reactions using chiral N-heterocyclic carbenes (NHCs) in conjunction with other catalysts. One of the very recent examples demonstrated a convenient strategy toward realizing chiral benzofuranones from salicylaldehyde and dimethyl acetylenedicarboxylate (DMAD). In this article, we report the mechanism and insights on the origin of asymmetric induction as obtained through a comprehensive density functional theory (M06-2X and mPW1K) investigation. Different likely catalyst−substrate combinations as well as the timing/sequence of activation of different substrates are carefully examined so as to identify the most preferred pathway. In the lowest energy path, the activation of DMAD by quinuclidine occurs first; the resulting zwitterionic intermediate then undergoes a Michael addition with a salicylate ion to yield a salicylate−DMAD adduct, which, in turn, is intercepted by the chiral NHC. In the next crucial step, an enantioselective C−C bond formation via an intramolecular Stetter reaction furnishes the benzofuranone framework bearing a chiral carbon atom. Two transition state models, with and without an explicitly bound catechol (an additive employed in the reaction that resulted in enhanced enantioselectivity), are considered. A distinct energetic advantage, of the order of 3.4 kcal/mol, for the addition of the *re* face of the Breslow intermediate (derived from the chiral NHC and the salicylate−DMAD adduct) to the *re* face of the dimethyl maleate moiety is noticed in the stereocontrolling C−C bond formation step. The Gibbs free energy difference between the diastereomeric transition states for (*re,re*) and (*re,si*) modes of addition is traced to the differential nonbonding interactions (O−H···π, lone pair (lp)···π, and C−H···O). The predicted enantioselectivity is in good agreement with the experimental observations.

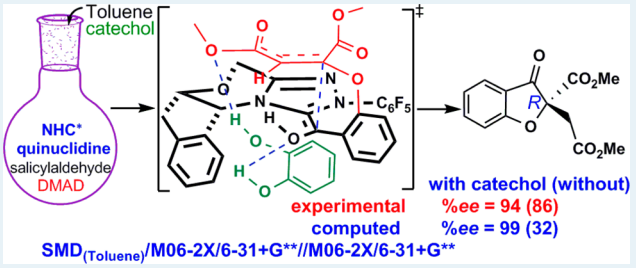

KEYWORDS: *asymmetric catalysis, transition state, N-heterocyclic carbenes, noncovalent interactions, Stetter reaction, dual catalysis, reaction mechanism*

INTRODUCTION

The use of N-heterocyclic carbenes as an asymmetric organocatalyst has been widely recognized for its utility in a diverse set of reactions. Nucleophilic NHCs have found applications in a number of expedient synthetic strategies in the recent times.[1] Although the earliest demonstrations on the potential of nucleophilic carbenes toward imparting umpolung reactivity can be traced to a few decades ago,[2] beginning from the mid 1990s, the domain of asymmetric NHC-catalyzed reactions has witnessed a renaissance.[3] In particular, pioneering contributions by Enders, Glorius, Nair, Rovis, Scheidt, Bode, Robin Chi, Lupton, and many others have helped engender considerable confidence on the potential of NHC as an effective organocatalyst.[4] Very recently, increasingly sophisticated examples of NHC catalysis, encompassing both cooperative and multicatalytic cascades have appeared.[5] All these developments should be regarded as a testimony to the continued success of NHC catalysis.

Akin to related organocatalytic reactions such as with secondary amines, the mechanistic studies on NHCs have invoked considerable recent interest.[6] Much of the attention has been devoted to the formation of nucleophilic Breslow intermediate and its reactions with a variety of acceptor molecules. In the recent past, we have established the importance of assisted proton transfer in Breslow intermediate formation as well as the mechanism of a few NHC-catalyzed reactions.[7] However, the mechanistic intricacies become increasingly more complex when other catalysts are employed in conjunction with the NHC in one-pot reaction conditions. Although development of efficient one-pot, multicatalytic cascades remains a formidable challenge owing to the compatibility issues between different catalysts, several clever methods have recently been proposed.

Adequate understanding of the mechanistic details would certainly help exploit the latent potential of multicatalytic cascades. In the present study, we aim to shed light on the

Received: December 13, 2014
Revised: January 28, 2015
Published: January 29, 2015

DOI: 10.1021/cs502006x
ACS Catal. 2015, 5, 1596−1603

mechanism and origin of enantioselectivity in an asymmetric Michael–Stetter cascade between salicylaldehyde and dimethyl acetylenedicarboxylate (DMAD), catalyzed by a chiral triazole-derived carbene in conjunction with quinuclidine (**Qn**) as the second catalyst (Scheme 1).[5e] The target compound obtained through this multicatalytic cascade, by itself, is an inherently interesting chiral benzofuranone. Benzofuran family of compounds have remained an important synthetic target owing to its potential as antifungal, anticancer, and antipsychotic activities.[8] Herein, we report some interesting mechanistic insights obtained through density functional theory investigation at the $SMD_{(Toluene)}$/M06-2X/6-31+G**//M06-2X/6-31+G** level of theory.

Scheme 1. Enantioselective Synthesis of Benzofuranones from Salicylaldehyde and DMAD Using a Catalytic Cascade by Qn and Chiral NHC (ref 5e)

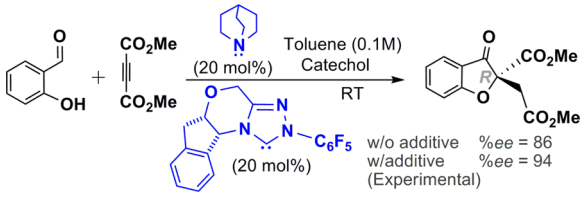

RESULTS AND DISCUSSION

The experimental approach employed by Rovis and co-workers involved the treatment of salicylaldehyde, dimethyl acetylenedicarboxylate (DMAD), **Qn** and a chiral triazolium salt as the carbene (NHC) precursor, all in one reaction vessel at room temperature in toluene.[5e] It is also interesting to note that the inclusion of catechol as an additive resulted in improved enantioselectivity. Because the reagents are mixed together with the catalysts in a one-pot reaction condition, the number of likely combinations between them can be envisaged to be proportionately higher as opposed to that in a sequential addition followed by synthetic manipulations of the intermediate compounds.

Depending on the sequence of combination between different reactants and the timing of the catalytic events, different mechanistic pathways are considered.[9] In this article, we wish to present only the energetically most favored pathway, chosen from among the different sequences of combination of reactants, responsible for the formation of the major product benzofuranone (**11**) and the key side product chromene (**17**), as outlined in Scheme 2. We further intend to convey that the mechanistic conclusions as to what is the most likely pathway in a multicatalytic one-pot reaction should rigorously consider a range of possibilities before accepting or discarding one on the basis of the computed energetics. A perusal of the contents provided in the Supporting Information is desirable toward appreciating what led to the choice of the mechanistic route as discussed here in the text. For the sake of brevity, the comprehensive details on the alternative pathways leading to different final products, other than benzofuranones, are placed in the second half of the Supporting Information.

The catalytic cycle involved in the formation of one of the key products (i.e., a salicylate intermediate **6**) begins with the addition of **Qn** to DMAD, as shown in Scheme 2. The zwitterionic intermediate **2** thus generated can abstract a proton from salicylaldehyde **3** to generate intermediate **4** and a salicylate ion. The activated double bond in **4** can act as a good Michael acceptor for the salicylate ion. The Michael adduct **5** generated upon the addition of salicylate can then expel **Qn**, leading to the formation of a salicylate intermediate **6** (Scheme 2).[10] The DMAD–salicylaldehyde Michael adduct **6** generated through the first catalytic cycle enters the second cycle of the reaction wherein it is intercepted by the chiral NHC, as shown

Scheme 2. Key Mechanistic Steps Involved in Asymmetric Michael–Stetter Cascade Reaction to Enantiomerically Enriched Benzofuranone (11)

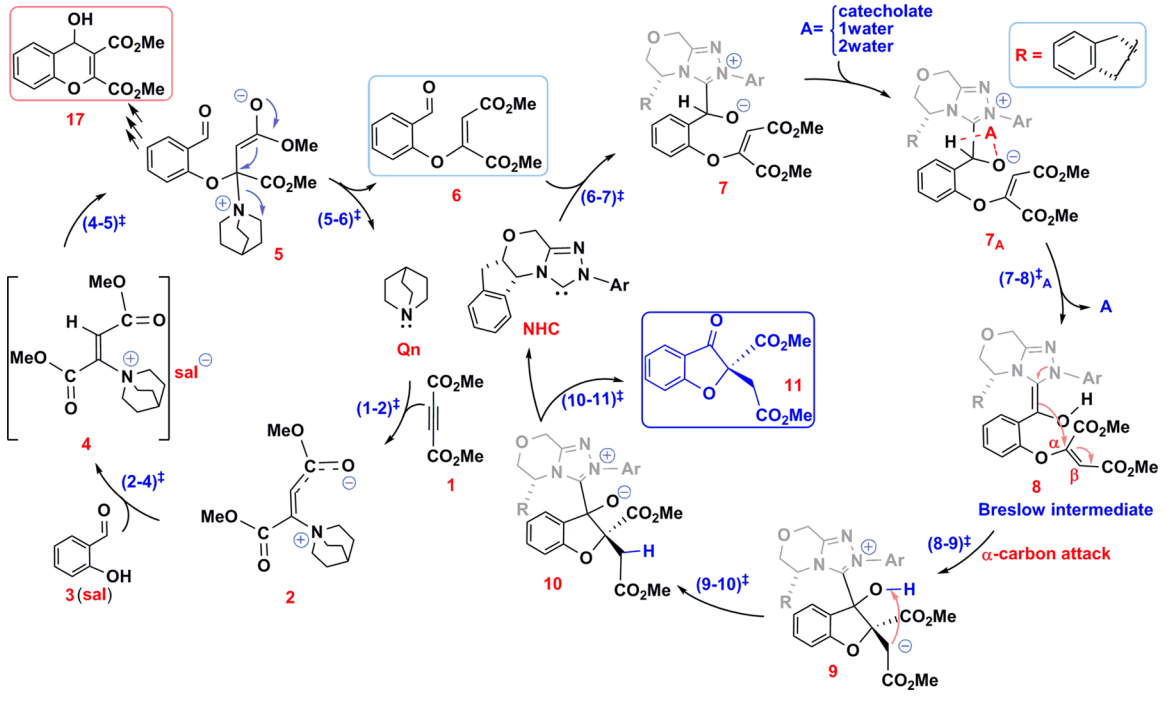

DOI: 10.1021/cs502006x
ACS Catal. 2015, 5, 1596–1603

in Scheme 2. The nucleophilic addition of NHC to the electrophilic carbonyl carbon of **6** gives a zwitterionic intermediate **7**. One of the most vital steps involved in organocatalytic reactions involving NHC is the formation of a Breslow intermediate. The intermediate **7** can, in principle, form a Breslow intermediate **8** via a three-membered proton transfer step. Subsequent intramolecular Michael addition in intermediate **8** leads to intermediate **9**.[11] Further intramolecular proton transfer through a five-membered ring **9** generates a tetrahedral intermediate **10**, which eventually furnishes benzofuranone product **11** with the release of the NHC.

To render improved clarity, the energetics of formation of **6** is presented first. The stereoselective step involving the action of chiral triazolinylidene NHC on **6** and the molecular origin of chiral induction is described next. The Gibbs free energy profile for the generation of intermediate **6**, as given in Figure 1,

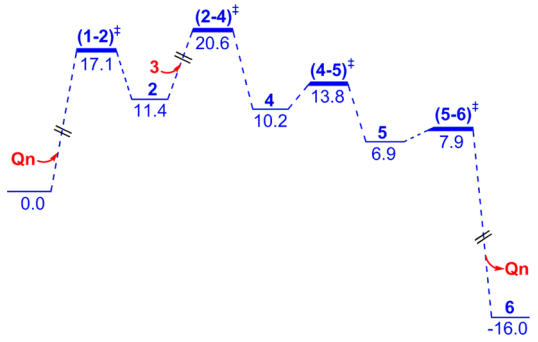

Figure 1. Gibbs free energy (kcal/mol) profile for the formation of salicylate intermediate **6** from DMAD and **Qn** obtained at the $SMD_{(Toluene)}$/M06-2X/6-31+G**//M06-2X/6-31+G** level of theory.

provides a number of important features of this catalytic cascade. A detailed sampling of the conformers arising due to different orientations of dimethyl maleate moiety as well as the *E* and *Z* configurations of the alkene is carried out (see Figure S2 in the Supporting Information for more details) to identify energetically the most preferred transition state.

The initial nucleophilic addition of **Qn** to the activated triple bond of DMAD via $(\mathbf{1-2})^{‡}$ involves a notable barrier about 17 kcal/mol. Most of the intermediates involved in the catalytic cycle triggered by **Qn** are found to be endoergic with respect to the separated reactants. The first zwitterionic intermediate **2** gets protonated by the incoming salicylaldehyde **3** via $(\mathbf{2-4})^{‡}$. The elementary step barrier is 9.2 kcal/mol for this protonation. The second Michael addition of the salicylate ion to the activated double bond of **4** exhibits only a low elementary step barrier of 3.6 kcal/mol. The different conformational and configurations possibilities that differ respectively in the orientations of the aldehyde group of the salicylate ion and across the C−C double bond of the quinuclidinium ion **4** are considered so as to identify the lowest energy transition state for $(\mathbf{4-5})^{‡}$.[12] The intermediate **5** thus produced can either expel **Qn**, as shown in Scheme 2, or undergo and intramolecular aldol cyclization with the aldehyde group of the salicylate. It is noticed that the barrier for the removal of **Qn** leading to product **6** via $(\mathbf{5-6})^{‡}$ is only about a kcal/mol. However, the corresponding barrier for aldol cyclization is about 9 kcal/mol, indicating a distinct kinetic advantage for the formation of **6**. Moreover, the generation of salicylate **6** is found to be exergonic by 16 kcal/mol. Thus, the energetically less favored aldol pathway, without the NHC participation, can account for the formation of a chromene (minor product).[9]

The next most important step in the reaction is the interception of salicylate **6** by the chiral NHC. As with the related NHC-catalyzed reactions, the formation of a Breslow intermediate between **6** and NHC is considered first.[13] The computed Gibbs free energies of all the key events involved in this catalytic cycle are provided in Figure 2. The barrier for the

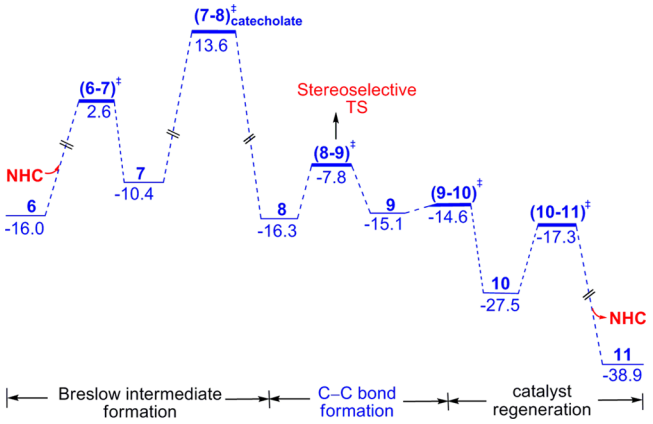

Figure 2. Gibbs free energy (kcal/mol) profile for the conversion of the salicylate intermediate **6** to benzofuranone product (**11**) by the action of NHC obtained at the $SMD_{(Toluene)}$/M06-2X/6-31+G**//M06-2X/6-31+G** level of theory.

C−C bond formation between the nucleophilic NHC and the aldehydic carbon atom of **6**, via $(\mathbf{6-7})^{‡}$, is 18.6 kcal/mol. On the other hand, the computed barriers for a direct 1,2-proton transfer in **7** is as high as 48 kcal/mol, which is in concert with earlier reports concerning the energetics of the Breslow intermediate formation.[7a−c,14] Hence, a two-step assisted-proton transfer, facilitated either by water or by catechol, is herein proposed. It is important to reckon that catechol is employed as an additive in the title reaction. A transition state for the proton transfer $(\mathbf{7-8})^{‡}$ enabled by a catecholate ion (obtained upon a favorable deprotonation by **Qn**) is identified as 24 kcal/mol lower in energy as compared to a direct 1,2-proton transfer. Similarly, a relay proton transfer, promoted by two explicit water molecules, is also found to be of similar energies as that of the catecholate-assisted proton transfer.[15] The formation of Breslow intermediate (**8**) is exoergic by 16.3 kcal/mol with respect to the separated reactants, indicating that with a suitable experimental probe the participation of **8** in the reaction could be detected.[16]

The most critical step in this reaction is an intramolecular Stetter reaction, wherein the nucleophilic Breslow intermediate adds to the activated maleate double bond. The addition to the α-carbon of the maleate moiety results in a furanoid ring as shown in **9** (Scheme 2). It can readily be noticed that both the donor and acceptor moieties involved in this ring-closing step offer prochiral faces. A total of eight stereochemically distinct modes for the C−C bond formation are therefore considered that differ in terms of the (i) *re* or *si* prochiral faces of the reacting partners and (ii) the ring conformation of the morpholine ring of the chiral NHC. As shown in Figure 3, when the morpholine oxygen is oriented downward toward the indane ring, it is termed as *cis*, and when it remains in an upward position, it is termed as *trans*. In addition to these

DOI: 10.1021/cs502006x
ACS Catal. 2015, 5, 1596−1603

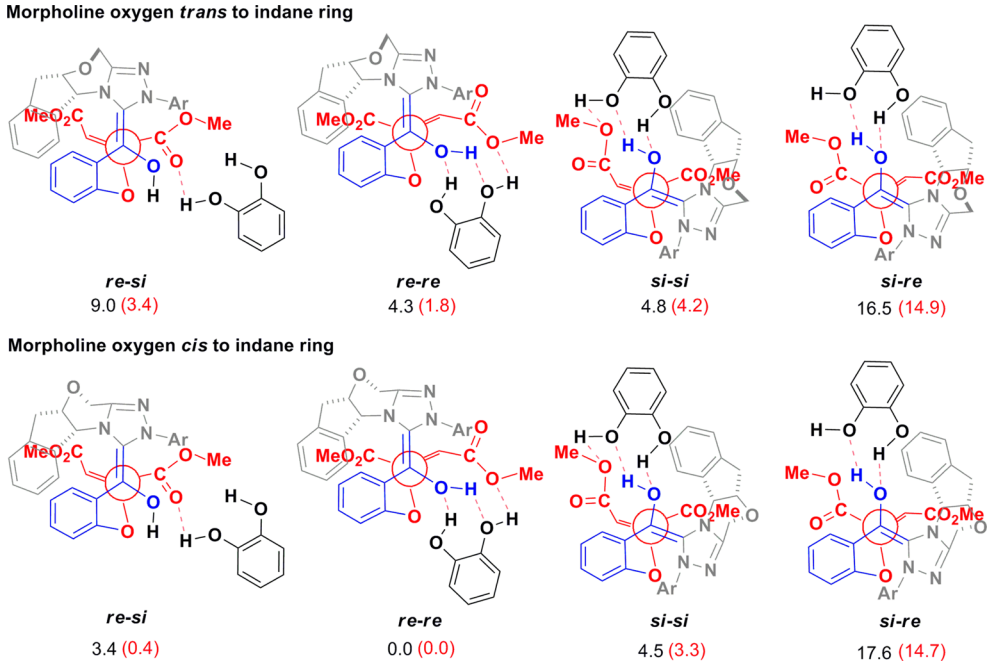

Figure 3. Different stereochemical possibilities involved in the stereoselectivity-controlling transition states for the C−C bond formation consisting of an explicitly included catechol. The Newman projection along the incipient C−C bond is shown. The relative energies at the $SMD_{(Toluene)}$/M06-2X/6-31+G**//M06-2X/6-31+G** are shown with respect to the lowest energy transition state. The values in parentheses refer to the values in the absence of the explicit catechol in the transition state.

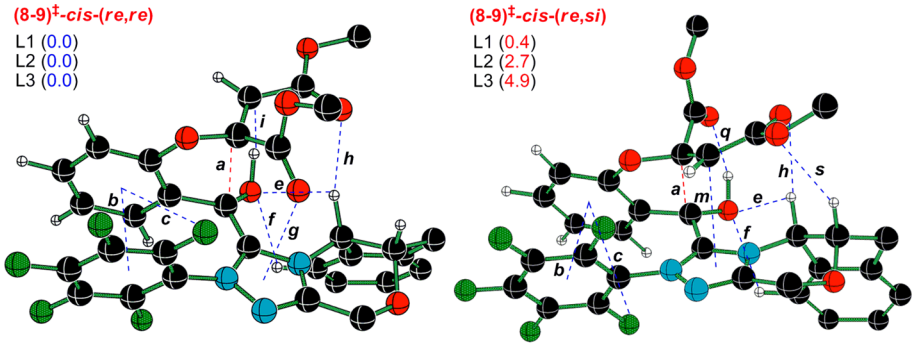

	a	*b*	*c*	*e*	*f*	*g*	*h*	*i*	*m*	*q*	*s*
***cis*-(*re*,*re*)**	2.23	2.99	2.94	2.45	2.42	2.73	2.26	2.08	–	–	–
***cis*-(*re*,*si*)**	2.03	3.01	3.00	2.41	2.43	–	2.39	–	2.96	1.77	2.51

Figure 4. Optimized geometries of the diastereomeric transition states at the M06-2X/6-31+G** level of theory for the enantioselective C−C bond formation in the absence of catechol. L1($SMD_{(Toluene)}$/M06-2X/6-31+G**//M06-2X/6-31+G**), L2($SMD_{(Toluene)}$/mPW1K/6-31+G**//mPW1K/6-31+G**), and L3($SMD_{(Toluene)}$/B3LYP/6-31+G**//B3LYP/6-31+G**). (C = black, N = cyan, O = red, F = green, H = gray). Note that the letters denoting noncovalent interactions are discontinuous here due to the lack of certain types of interactions as compared to those in Figure 5 where it is continuous.

stereochemical possibilities, we have also identified the stereocontrolling transition states with and without an explicitly included catechol. This has been done in view of an increase in enantioselectivity noticed by Rovis and co-workers when catechol was employed as an additive.[5e,17]

The computed relative Gibbs free energies of the C−C bond formation transition states, with and without an explicit molecule of catechol, along with their broad stereochemical features are provided in Figure 3.[18] In the absence of the catechol, the addition of the *re* face of enol to the *re* face of the maleate with a *cis* conformation of the morpholine oxygen is computed as the lowest energy mode. This transition state, designated as *cis*-(***re*,*re***), corresponds to the product with a *R* configuration for the newly generated chiral carbon atom, which is in line with the sense of enantioselectivity reported experimentally.[5e] However, the difference in Gibbs free energy between the diastereomeric transition states, *cis*-(***re*,*re***) and *cis*-(***re*,*si***), which is responsible for the extend of stereoselectivity, is found to be only 0.4 kcal/mol.[19] Because the predicted enantioselectivity is much lower than the experimental value, we have examined the geometric features more closely, both in the gas phase and in the condensed phase. Full geometry optimization of these transition states, in a toluene continuum, again yielded an energy difference of only 0.9 kcal/mol. The origin of such a modest energy difference is traced to the lack of differential in the intramolecular interactions. For instance, the

DOI: 10.1021/cs502006x
ACS Catal. 2015, 5, 1596−1603

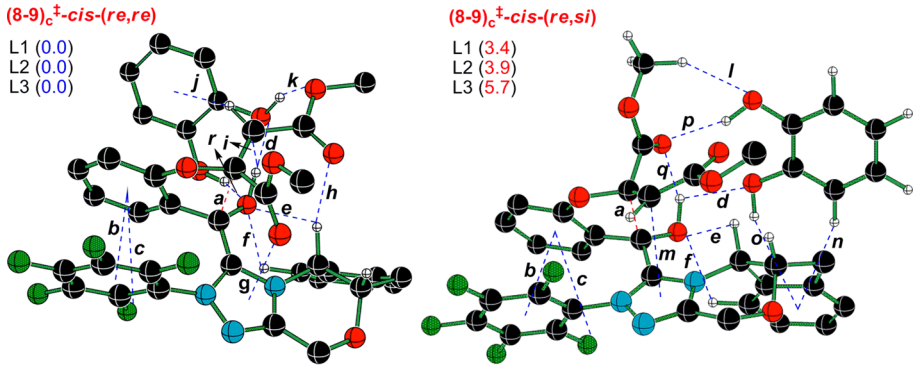

	a	b	c	d	e	f	g	h	i
cis-(re,re)$_c$	2.27	2.99	2.96	2.10	2.44	2.45	2.72	2.38	2.14
cis-(re,si)$_c$	2.02	3.02	3.02	2.22	2.44	2.38	–	–	–

	j	k	l	m	n	o	p	q	r
cis-(re,re)$_c$	2.79	1.95	–	–	–	–	–	–	2.08
cis-(re,si)$_c$	–	–	2.52	2.85	2.76	2.62	1.99	1.77	–

Figure 5. Optimized diastereomeric transition states at the M06-2X/6-31+G** level of theory for the enantioselective C−C bond formation in the presence of catechol. The bond lengths are in Å. The values in parentheses are relative Gibbs free energies at L1(SMD$_{(Toluene)}$/M06-2X/6-31+G**//M06-2X/6-31+G**), L2(SMD$_{(Toluene)}$/mPW1K/6-31+G**//mPW1K/6-31+G**), and L3(SMD$_{(Toluene)}$/B3LYP/6-31+G**//B3LYP/6-31+G**). (C = black, N = cyan, O = red, F = green, H = gray).

noncovalent interactions (denoted as *a-s*, in Figure 4) in *cis*-(***re,re***) and *cis*-(***re,si***) are closely similar in these diastereomeric transition states.[20]

Another transition state model with an explicitly included catechol is then examined wherein it participates in hydrogen bonding interactions with the enol and the maleate oxygen atoms (Figure 3). Again, the energetically most preferred transition state is found to be *cis*-(***re,re***)$_c$ similar to that noted in the absence of catechol. The subscript "c" here denotes that these transition states contain an explicit catechol molecule. The most important aspect of this refined transition state model with an explicit catechol is that the difference in Gibbs free energy between the stereocontrolling diastereomeric transition states *cis*-(***re,re***)$_c$ and *cis*-(***re,si***)$_c$ is 3.4 kcal/mol.[21] Such a pronounced energy separation corresponds to % ee of 99, which is in excellent agreement with the experimentally reported value.[5e] This prediction is again in concert with the fact that the inclusion of catechol as an additive resulted in an improvement in the observed enantioselectivity.

The analysis of the optimized geometries revealed that the hydrogen bonding interaction with catechol is vital toward providing an additional stabilization to the lower energy transition state *cis*-(***re,re***)$_c$. Improved noncovalent interactions between the catechol and the substrates in *cis*-(***re,re***)$_c$ appear to have a direct impact as well. These interactions are mapped in Figure 5. Such additional stabilization results in a larger energy separation of 3.4 kcal/mol between the stereocontrolling transition states as opposed to a very narrow separation (0.4 kcal/mol) in the absence of an explicit catechol. The stereocontrolling factors operating in the transition states are carefully analyzed to understand the origin of chiral induction. As depicted in Figure 5, a number of crucial noncovalent contacts[22] are identified, which include (i) $\pi\cdots\pi$ interaction (*b* and *m*), (ii) C−H···O (*e*, *f*, *h*, and *l*) and O−H···O hydrogen bonding (*d*, *k*, *p*, *q*, and *r*), (iii) lone pair (lp)$\cdots\pi$ interaction (*g*), (iv) C−H$\cdots\pi$ interaction (*n*, and *j*), (v) O−H$\cdots\pi$ interaction (*i*, and *o*), and (vi) C−F$\cdots\pi$ interaction (*c*). These interactions are further probed by evaluating the electron densities at the bond critical points along the respective bond paths within the quantum theory of Atoms-In-Molecule (AIM) formalism.[23] The interactions that render additional stabilization to the lower energy transition state *cis*-(***re,re***)$_c$ are (i) a stronger O−H$\cdots\pi$ interaction (*i*, 2.14 Å) than *cis*-(***re,si***)$_c$ (*o*, 2.62 Å),[24] (ii) lone pair (lp)$\cdots\pi$ interaction (*g*) which is present in *cis*-(***re,re***)$_c$ but is absent in *cis*-(***re,si***)$_c$ and (iii) a moderately stronger C−H···O (*e*, *f*, and *h*) interaction in *cis*-(***re,re***)$_c$ than in *cis*-(***re,si***)$_c$.[25]

Through the stereocontrolling Stetter reaction (C−C bond formation) as described above, the benzofuranone framework is built with a chiral carbon atom. In the ensuing steps, the generated ester enolate intermediate **9** will undergo a protonation. The geometry of **9** is such that hydroxyl group is suitably poised for a five-member proton transfer transition state. The intramolecular proton transfer provides a tetrahedral alkoxide intermediate **10** via a low energy transition state (**9**−**10**)‡ (Figure 2). The barrier for the catalyst regeneration and product release, calculated as the difference in Gibbs free energies between transition state (**10**−**11**)‡ and the alkoxide intermediate **10**, is 10.2 kcal/mol. The overall reaction is estimated as exergonic by about 39 kcal/mol for the formation of the final product **11** ((*R*)-methyl 2-(2-methoxy-2-oxoethyl)-3-oxo-2,3-dihydrobenzofuran-2-carboxylate).

An interesting aspect relating to the asymmetric induction as described above is that the enantiocontrol is exerted by a network of noncovalent interactions between the catalyst and the reacting substrates. These very interactions could, in principle, be exploited as a handle for steering the stereochemical course of the reaction through catalyst/substrate modifications. For instance, the $\pi\cdots\pi$ stacking interaction between the *N*-aryl(C_6F_5) group and salicylaldehyde moiety (*b* and *c*) and C−H$\cdots\pi$ interactions (*n* and *j*) are quite similar in both diastereomeric *cis*-(***re,re***)$_c$ and *cis*-(***re,si***)$_c$ transition states (Figure 5). To examine the role of the pentafluoroaryl decoration on the triazolium moiety, we have systematically modified the *N*-aryl group by a suitably chosen set of substituents.[26] Most significantly, the predicted % ee is found to be the best for the parent C_6F_5 group as compared to its

DOI: 10.1021/cs502006x
ACS Catal. 2015, 5, 1596−1603

modified aryl substituents. For instance, with modified aryl groups the predicted % ee are 64 (C_6H_5), 91 (2,6-$F_2C_6H_3$), 98 (2,4,6-$Cl_3C_6F_2$), 97 (2,4,6-$Cl_3C_6H_2$), 91 (2,4,6-$Me_3C_6H_2$), 94 (2-Me,4-$MeOC_6H_3$), suggesting a direct role of the pentafluoroaryl group.

CONCLUSIONS

The mechanism of a multicatalytic asymmetric Michael−Stetter cascade reaction between salicylaldehyde and DMAD has been established by using DFT (M06-2X and mPW1K) computational methods. The role of **Qn** has been identified as responsible for the activation of DMAD toward its reaction with a salicylate ion, to eventually furnish salicylate−DMAD adduct. The chiral NHC intercepts the salicylate generated through the first **Qn**-catalyzed cycle to form a Breslow intermediate. The catechol additive has been found to play a vital role in lowering the activation barrier both for the Breslow intermediate formation and in the subsequent enantioselective C−C bond formation leading to the benzofuran framework. The intramolecular addition of the *re* face of the enol on the *re* face of α-carbon of the maleate moiety has been noted as the most preferred mode for the C−C bond formation. The computed % ee in this intramolecular Stetter reaction is in good agreement with experimental value in the presence of catechol. The origin of asymmetric induction stems from the differences in O−H···π, lone pair···π, and C−H···O nonbonding interactions between the stereocontrolling transition states.

COMPUTATIONAL METHODS

DFT (density functional theory) calculations on all the stationary points such as intermediates, reactants, and transition states were carried out using M06-2X[27] and mPW1K[28] functional. In addition to using these two functionals, the B3LYP[29] computations were also carried out for the stereoselective C−C bond formation all in conjunction with the Pople basis set 6-31+G**.[30] Fully optimized geometries of all the stationary points were characterized by frequency calculations in order to verify that (a) the transition states (TSs) have one and only one imaginary frequency pertaining to the desired reaction coordinate, and (b) all minimum energy structures have only positive Hessian matrix. The Intrinsic Reaction Coordinate (IRC) calculations were performed at the mPW1K and M06-2X levels of theory to further authenticate that the TS on the energy profiles connect to the desired minima on either side of the first order saddle point. These geometries were further optimized by using "opt = calcfc" key word. Gibbs free energies were obtained by adding the thermal and entropic terms estimated by using standard statistical mechanical approximations (rigid rotor and harmonic vibrational frequencies) at 298.15K and 1 atm pressure. All calculations were carried out using the Gaussian 09 suite of quantum chemical program.[31]

The effect of continuum solvation was incorporated by using the SMD solvation model wherein the full solute electron density is employed without defining partial atomic charges as well as an universal solvation model.[32] The single point energy calculations were carried out in the condensed phase, on the gas phase geometries obtained at the M06-2X and mPW1K level of theory with 6-31+G** basis set. Because the experimental studies employed toluene as a solvent, we have employed the continuum dielectric of toluene (dielectric constant, ε = 2.37). The Gibbs free energies and enthalpies for all stationary points in the condensed phase were obtained by adding the corresponding thermal energies obtained in the gas phase computations to the single point energies. The full geometry optimizations were carried out at the $SMD_{(Toluene)}$/M06-2X/6-31+G** level of theory for the four of eight diastereomeric TSs (which are lowest energy TSs in the presence and absence of catechol) leading to enantiomeric products. The Gibbs free energies provided in the text are at the $SMD_{(Toluene)}$/M06-2X/6-31+G**//M06-2X/6-31+G** level of theory for all the stationary points.

ASSOCIATED CONTENT

Supporting Information

The following file is available free of charge on the ACS Publications website at DOI: 10.1021/cs502006x.

Schemes and energetics of additional higher energy mechanistic pathways, optimized Cartesian coordinates of all the stationary points, and mapping of noncovalent interactions (PDF)

AUTHOR INFORMATION

Corresponding Author

*E-mail: sunoj@chem.iitb.ac.in.

Notes

The authors declare no competing financial interest.

ACKNOWLEDGMENTS

We acknowledge the computing time from the IIT Bombay supercomputing and Prof. Tomislav Rovis (Colorado State University) for some valuable discussions.

REFERENCES

(1) (a) Hopkinson, M. N.; Richter, C.; Schedler, M.; Glorius, F. *Nature* **2014**, *510*, 485−496. (b) Ryan, S. J.; Candish, L.; Lupton, D. W. *Chem. Soc. Rev.* **2013**, *42*, 4906−4917. (c) Bugaut, X.; Glorius, F. *Chem. Soc. Rev.* **2012**, *41*, 3511−3522. (d) Izquierdo, J.; Huston, G. E.; Cohen, D. T.; Scheidt, K. A. *Angew. Chem., Int. Ed.* **2012**, *51*, 11686−11698. (e) Vora, H. M.; Rovis, T. *Aldrichimica Acta* **2011**, *44*, 3−11. (f) Phillips, E. M.; Chan, A.; Scheidt, K. A. *Aldrichimica Acta* **2009**, *42*, 55−66. (g) Nair, V.; Menon, R. S.; Biju, A. T.; Sinu, C. R.; Paul, R. R.; Jose, A.; Sreekumar, V. *Chem. Soc. Rev.* **2011**, *40*, 5336−5346. (h) Enders, D.; Niemeier, O.; Henseler, A. *Chem. Rev.* **2007**, *107*, 5606−5655. (i) Marion, N.; Diez-Gonzalez, S.; Nolan, S. P. *Angew. Chem., Int. Ed.* **2007**, *46*, 2988−3000.

(2) Breslow, R. *J. Am. Chem. Soc.* **1958**, *80*, 3719−3726.

(3) (a) Bourissou, D.; Guerret, O.; Gabbaï, F. P.; Bertrand, G. *Chem. Rev.* **2000**, *100*, 39−91. (b) Knight, R. L.; Leeper, F. J. *Tetrahedron Lett.* **1997**, *38*, 3611−3614. (c) Enders, D.; Breuer, K.; Teles, J. H. *Helv. Chim. Acta* **1996**, *79*, 1217−1221. (d) Enders, D.; Breuer, K.; Runsink, J.; Teles, J. H. *Helv. Chim. Acta* **1996**, *79*, 1899−1902.

(4) (a) Ni, Q.; Zhang, H.; Grossmann, A.; Loh, C. C. J.; Merkens, C.; Enders, D. *Angew. Chem., Int. Ed.* **2013**, *52*, 13562−13566. (b) Jousseaume, T.; Wurz, N. E.; Glorius, F. *Angew. Chem., Int. Ed.* **2011**, *50*, 1410−1414. (c) Guo, C.; Schedler, M.; Daniliuc, C. G.; Glorius, F. *Angew. Chem., Int. Ed.* **2014**, *53*, 10232−10236. (d) Nair, V.; Sreekumar, V.; Manojkumar, P.; Mohan, R.; Suresh, E. *J. Am. Chem. Soc.* **2006**, *128*, 8736−8737. (e) DiRocco, D. A.; Noey, E. L.; Houk, K. N.; Rovis, T. *Angew. Chem., Int. Ed.* **2012**, *51*, 2391−2394. (f) DiRocco, D. A.; Rovis, T. *J. Am. Chem. Soc.* **2011**, *133*, 10402−10405. (g) de Alaniz, J. R.; Rovis, T. *J. Am. Chem. Soc.* **2005**, *127*, 6284−6289. (h) Lee, A.; Younai, Y.; Price, C. K.; Izquierdo, J.; Mishra, R. K.; Scheidt, K. A. *J. Am. Chem. Soc.* **2014**, *136*, 10589−10592. (j) Phillips, E. M.; Riedrich, M.; Scheidt, K. A. *J. Am. Chem. Soc.* **2010**, *132*, 13179−13181. (k) Kravina, A. G.; Mahatthananchai, J.; Bode, J. W. *Angew. Chem., Int. Ed.* **2012**, *51*, 9433−9436. (l) Zhang, J.; Xing,

DOI: 10.1021/cs502006x
ACS Catal. 2015, 5, 1596−1603

C.; Tiwari, B.; Chi, Y. R. *J. Am. Chem. Soc.* **2013**, *135*, 8113−8116. (n) Zhu, T.; Zheng, P.; Mou, C.; Yang, S.; Song, B.-A.; Chi, Y. R. *Nature Commun.* **2014**, *5*, 5027. (o) Candish, L.; Lupton, D. W. *J. Am. Chem. Soc.* **2013**, *135*, 58−61. (p) Han, R.; Qi, J.; Gu, J.; Ma, D.; Xie, X.; She, X. *ACS Catal.* **2013**, *3*, 2705−2709. (r) Yang, L.; Wang, F.; Lee, R.; Lv, Y.; Huang, K.-W.; Zhong, G. *Org. Lett.* **2014**, *16*, 3872−3875. (s) Zhao, M.; Yang, H.; Li, M.-M.; Chen, J.; Zhou, L. *Org. Lett.* **2014**, *16*, 2904−2907. (t) Rafiński, Z.; Kozakiewicz, A.; Rafiński, K. *ACS Catal.* **2014**, *4*, 1404−1408.

(5) (a) Grossmann, A.; Enders, D. *Angew. Chem., Int. Ed.* **2012**, *51*, 314−325. (b) Izquierdo, J.; Orue, A.; Scheidt, K. A. *J. Am. Chem. Soc.* **2013**, *135*, 10634−10637. (c) Cohen, D. T.; Scheidt, K. A. *Chem. Sci.* **2012**, *3*, 53−57. and references therein. (d) Lathrop, S. P.; Rovis, T. *J. Am. Chem. Soc.* **2009**, *131*, 13628−13630. (e) Filloux, C. M.; Lathrop, S. P.; Rovis, T. *Proc. Natl. Acad. Sci. U.S.A.* **2010**, *107*, 20666−20671. (g) Biju, A. T.; Wurz, N. E.; Glorius, F. *J. Am. Chem. Soc.* **2010**, *132*, 5970−5971. (h) Jiang, H.; Gschwend, B.; Albrecht, Ł.; Jørgensen, K. A. *Org. Lett.* **2010**, *12*, 5052−5055. (i) Anwar, S.; Chang, H.-J.; Chen, K. *Org. Lett.* **2011**, *13*, 2200−2203. (j) Zhao, X.; DiRocco, D. A.; Rovis, T. *J. Am. Chem. Soc.* **2011**, *133*, 12466−12469. (k) Mo, J.; Chen, X.; Chi, Y. R. *J. Am. Chem. Soc.* **2012**, *134*, 8810−8813. (l) Jin, Z.; Xu, J.; Yang, S.; Song, B.-A.; Chi, Y. R. *Angew. Chem., Int. Ed.* **2013**, *52*, 12354−12358. (m) Xiao, Z.; Yu, C.; Li, T.; Wang, X.-S.; Yao, C. *Org. Lett.* **2014**, *16*, 3632−3635. (o) Namitharan, K.; Zhu, T.; Cheng, J.; Zheng, P.; Li, X.; Yang, S.; Song, B.-A.; Chi, Y. R. *Nature Commun.* **2014**, *5*, 3982. (p) Bera, S.; Samanta, R. C.; Daniliuc, C. G.; Studer, A. *Angew. Chem., Int. Ed.* **2014**, *53*, 9622−9626. (q) Liu, K.; Hovey, M. T.; Scheidt, K. A. *Chem. Sci.* **2014**, *5*, 4026−4031. (r) Lee, A.; Scheidt, K. A. *Angew. Chem., Int. Ed.* **2014**, *53*, 7594−7598.

(6) (a) Um, J. M.; DiRocco, D. A.; Noey, E. L.; Rovis, T.; Houk, K. N. *J. Am. Chem. Soc.* **2011**, *133*, 11249−11254. (b) Domingo, L. R.; Aurell, M. J.; Arno, M. *Tetrahedron* **2009**, *65*, 3432−3440. (c) Domingo, L. R.; Zaragoza, R. J.; Arno, M. *Org. Biomol. Chem.* **2010**, *8*, 4884−4891. (d) Domingo, L. R.; Zaragozá, R. J.; Saéz, J. A.; Arnó, M. *Molecules* **2012**, *17*, 1335−1353. (e) Li, Z.; Wei, D.; Wang, Y.; Zhu, Y.; Tang, M. *J. Org. Chem.* **2014**, *79*, 3069−3078. (f) Johnston, R. C.; Cohen, D. T.; Eichman, C. C.; Scheidt, K. A.; Cheong, P. H.-Y. *Chem. Sci.* **2014**, *5*, 1974−1982. (g) Mahatthananchai, J.; Bode, J. W. *Acc. Chem. Res.* **2014**, *47*, 696−707. (h) Allen, S. E.; Mahattananchai, J.; Bode, J. W.; Kozlowski, M. C. *J. Am. Chem. Soc.* **2012**, *34*, 12098−12103. (i) Hawkes, K. J.; Yates, B. F. *Eur. J. Org. Chem.* **2008**, 5563−5570.

(7) (a) Reddi, Y.; Sunoj, R. B. *Org. Lett.* **2012**, *14*, 2810−2813. (b) Verma, P.; Patni, P. A.; Sunoj, R. B. *J. Org. Chem.* **2011**, *76*, 5606−5613. (c) Kuniyil, R.; Sunoj, R. B. *Org. Lett.* **2013**, *15*, 5040−5043. (d) Verma, P.; Verma, P.; Sunoj, R. B. *Org. Biomol. Chem.* **2014**, *12*, 2176−2179.

(8) (a) Pirrung, M. C.; Brown, W. L.; Rege, S.; Laughton, P. *J. Am. Chem. Soc.* **1991**, *113*, 8561−8562. (b) Charrier, C.; Clarhaut, J.; Gesson, J.−P.; Estiu, G.; Wiest, O.; Roche, J.; Bertrand, P. *J. Med. Chem.* **2009**, *52*, 3112−3115. (c) Sheng, R.; Xu, Y.; Hu, C.; Zhang, J.; Lin, X.; Li, J.; Yang, B.; He, Q.; Hu, Y. *Eur. J. Med. Chem.* **2009**, *44*, 7−17.

(9) Additional possible pathways, leading to products such as chromene, furanone and oxy-maleates, have been computed in great detail. The details provided in Part 2 of the Supporting Information (See Schemes S1−S7, Figures S18−S33, and Tables S12−S19).

(10) An alternative Baylis−Hillman pathway facilitated by an intramolecular aldol reaction in 5 can result in another intermediate, which upon a favorable base-assisted proton transfer and elimination of **Qn** can provide a chromene product. This pathway was found to be of higher energy. Further details are provided in Scheme S4 and Figure S27 in the Supporting Information.

(11) Different products (**11** and **14**) and different stereochemical pathways are found based on intramolecular Michael addition between the enol carbon and two distinct prochiral carbons such as α-carbon and β-carbon of maleate. Although Michael addition at the α prochiral carbon leads to product **11** with one quaternary stereocenter, addition to the β prochiral carbon leads to product **14** as shown in Scheme S3. Additional details on the energetics are provided in Tables S11 and S13 in the Supporting Information. The key optimized TSs are provided in Figures S17, S19, and S20 in the Supporting Information.

(12) The optimized transition state geometries as well as description of these geometric possibilities for all these steps are provided in Figures S2−S7 in the Supporting Information.

(13) (a) Nair, V.; Bindu, S.; Sreekumar, V.; Rath, N. P. *Org. Lett.* **2003**, *5*, 665−667. (b) de Alaniz, J. R.; Kerr, M. S.; Moore, J. L.; Rovis, T. *J. Org. Chem.* **2008**, *73*, 2033−2040.

(14) Examples on relay proton transfer see Sunoj, R. B.; Anand, M. *Phys. Chem. Chem. Phys.* **2012**, *14*, 12715−12736.

(15) See Figures S9−S10 and Table S11 in the Supporting Information for additional details.

(16) (a) Berkessel, A.; Elfert, S.; Yatham, V. R.; Neudörfl, J.-M.; Schlörer, N. E.; Teles, J. H. *Angew. Chem., Int. Ed.* **2012**, *51*, 12370−12374. (b) Berkessel, A.; Yatham, V. R.; Elfert, S.; Neudörfl, J.-M. *Angew. Chem., Int. Ed.* **2013**, *52*, 11158−11162.

(17) Explicit inclusion of solvents or additives in the transition states can be vital toward arriving at the correct stereochemical outcome of a given reaction. For example (a) Patil, M. P.; Sunoj, R. B. *Chem.—Eur. J.* **2008**, *14*, 10472−10485. (b) Sreenithya, A.; Sunoj, R. B. *Org. Lett.* **2012**, *14*, 5752−5755.

(18) Additional details of these TSs are provided in Table S5 in the Supporting Information.

(19) Meticulous care has been taken to confirm that such precariously low energy difference between the diastereomeric transition states is reliable within the affordable accuracy. A detailed conformational analysis of *cis*-(***re,re***) and *cis*-(***re,si***) transition states has been undertaken to verify that the energy difference indeed modest is the present case (Figure S12 in the Supporting Information).

(20) Geometries were also optimized at the mPW1K/6-31+G** and B3LYP/6-31+G** levels of theory to find that some of the noncovalent interactions such as C−F···π interaction and C-H···O hydrogen bonding interaction (respectively denoted as *c* and *s*) are weaker in the higher energy transition state *cis*-(***re,si***) culminating in to more destabilization of the transition state as compared to that at the M06-2X. Hence, a larger energy separation between *cis*-(***re,re***) and *cis*-(***re,si***) at both mPW1K and B3LYP functionals are noted. The enantioselectivity predicted at the $SMD_{(Toluene)}$/mPW1K/6-31+G**//mPW1K/6-31+G** and the $SMD_{(Toluene)}$/B3LYP/6-31+G**//B3LYP/6-31+G** level of theories are more than 98% (Table S6 in the Supporting Information).

(21) Whereas the imaginary frequency pertaining to the desired reaction coordinate is the most prominent one, an intruder imaginary frequency could not be eliminated in spite of repeated attempts. For example, see references (a) Wheeler, S. E.; McNeil, A. J.; Muller, P.; Swager, T. M.; Houk, K. N. *J. Am. Chem. Soc.* **2010**, *132*, 3304−3311. (b) Watt, M.; Hardebeck, L. K. E.; Kirkpatrick, C. C.; Lewis, M. *J. Am. Chem. Soc.* **2011**, *133*, 3854−3862.

(22) (a) Egli, M.; Sarkhel, S. *Acc. Chem. Res.* **2007**, *40*, 197−205. (b) Gung, B. W.; Zou, Y.; Xu, Z.; Amicangelo, J. C.; Irwin, D. G.; Ma, S.; Zhou, H.-C. *J. Org. Chem.* **2008**, *73*, 689−693. (c) Sarkhel, S.; Rich, A.; Egli, M. *J. Am. Chem. Soc.* **2003**, *125*, 8998−8999. (d) Hunter, C. A.; Sanders, J. K. M. *J. Am. Chem. Soc.* **1990**, *112*, 5525−5534. (e) Lu, Y.-X.; Zou, J.-W.; Wang, Y.-H.; Yu, Q.-S. *Int. J. Quantum Chem.* **2007**, *107*, 1479−1486. (f) Wheeler, S. *Acc. Chem. Res.* **2013**, *46*, 1029−1038. (g) Jindal, G.; Sunoj, R. B. *Angew. Chem., Int. Ed.* **2014**, *53*, 4432−4435.

(23) (a) Bond paths, bond critical points and the corresponding electron densities, as obtained using AIM topological analysis, are shown in Figure S16 and Table S8 in the Supporting Information.. (b) A description and comparison of these interactions are also provided in the accompanying text..

(24) (a) Kumari, M.; Balaji, P. V.; Sunoj, R. B. *Phys. Chem. Chem. Phys.* **2011**, *13*, 6517−6530. (b) Kumari, M.; Sunoj, R. B.; Balaji, P. V. *Org. Biomol. Chem.* **2012**, *10*, 4186−4200.

(25) All interactions which are vital to the transition state stabilization are shown in the figure.

DOI: 10.1021/cs502006x
ACS Catal. 2015, 5, 1596−1603

(26) (a) These computations were done at the mPW1K/6-31+G** level of theory in the absence of an explicit catechol in the transition state.. (b) See Table S7 in the Supporting Information for additional details..
(27) Zhao, Y.; Truhlar, D. G. *J. Chem. Phys.* **2006**, *125*, 194101−194118.
(28) (a) Lynch, B. J.; Fast, P. L.; Harris, M.; Truhlar, D. G. *J. Phys. Chem. A* **2000**, *104*, 4811−4815. (b) Lynch, B. J.; Zhao, Y.; Truhlar, D. G. *J. Phys. Chem. A* **2003**, *107*, 1384−1388.
(29) (a) Becke, A. D. *Phys. Rev. A* **1988**, *38*, 3098−3100. (b) Becke, A. D. *J. Chem. Phys.* **1993**, *98*, 5648−5652. (c) Lee, C. T.; Yang, W.; Parr, R. G. *Phys. Rev. B* **1988**, *37*, 785−789.
(30) Hariharan, P. C.; Pople, J. A. *Theor. Chim. Acta* **1973**, *28*, 213−222.
(31) Frisch, M. J.; Trucks, G. W.; Schlegel, H. B.; Scuseria, G. E.; Robb, M. A.; Cheeseman, J. R.; Scalmani, G.; Barone, V.; Mennucci, B.; Petersson, G. A.; Nakatsuji, H.; Caricato, M.; Li, X.; Hratchian, H. P.; Izmaylov, A. F.; Bloino, J.; Zheng, G.; Sonnenberg, J. L.; Hada, M.; Ehara, M.; Toyota, K.; Fukuda, R.; Hasegawa, J.; Ishida, M.; Nakajima, T.; Honda, Y.; Kitao, O.; Nakai, H.; Vreven, T.; Montgomery, Jr., J. A.; Peralta, J. E.; Ogliaro, F.; Bearpark, M.; Heyd, J. J.; Brothers, E.; Kudin, K. N.; Staroverov, V. N.; Kobayashi, R.; Normand, J.; Raghavachari, K.; Rendell, A.; Burant, J. C.; Iyengar, S. S.; Tomasi, J.; Cossi, M.; Rega, N.; Millam, N. J.; Klene, M.; Knox, J. E.; Cross, J. B.; Bakken, V.; Adamo, C.; Jaramillo, J.; Gomperts, R.; Stratmann, R. E.; Yazyev, O.; Austin, A. J.; Cammi, R.; Pomelli, C.; Ochterski, J. W.; Martin, R. L.; Morokuma, K.; Zakrzewski, V. G.; Voth, G. A.; Salvador, P.; Dannenberg, J. J.; Dapprich, S.; Daniels, A. D.; Farkas, Ö.; Foresman, J. B.; Ortiz, J. V.; Cioslowski, J.; Fox, D. J. *Gaussian 09*, Revision A.02; Gaussian, Inc.: Wallingford, CT, 2009.
(32) Marenich, A. V.; Cramer, C. J.; Truhlar, D. G. *J. Phys. Chem. B* **2009**, *113*, 6378−6396.

DOI: 10.1021/cs502006x
ACS Catal. 2015, 5, 1596−1603